Protein Inhibitors of Serine Proteinases: Role of Backbone Structure and Dynamics in Controlling the Hydrolysis Constant‡

Jikui Song and John L. Markley*

National Magnetic Resonance Facility, Department of Biochemistry, University of Wisconsin−Madison, 433 Babcock Drive, Madison, Wisconsin 53706

Received January 9, 2003; Revised Manuscript Received February 24, 2003

ABSTRACT: Standard mechanism protein inhibitors of serine proteinases bind as substrates and are cleaved by cognate proteinases at their reactive sites. The hydrolysis constant for this cleavage reaction at the P_1−P_1' peptide bond (K_{hyd}) is determined by the relative concentrations at equilibrium of the "intact" (uncleaved, I) and "modified" (reactive site cleaved, I*) forms of the inhibitor. The pH dependence of K_{hyd} can be explained in terms of a pH-independent term, $K_{hyd}°$, plus the proton dissociation constants of the newly formed amino and carboxylate groups at the cleavage site. Two protein inhibitors that differ from one another by a single residue substitution have been found to have $K_{hyd}°$ values that differ by a factor of 5 [Ardelt, W., and Laskowski, M., Jr. (1991) *J. Mol. Biol. 220*, 1041−1052]: turkey ovomucoid third domain (OMTKY3) has $K_{hyd}° = 1.0$, and Indian peafowl ovomucoid third domain (OMIPF3), which differs from OMTKY3 by the substitution P_2'-Tyr^{20}His, has $K_{hyd}° = 5.15$. What mechanism is responsible for this small difference? Is it structural (enthalpic) or dynamic (entropic)? Does the mutation affect the free energy of the I state, the I* state, or both? We have addressed these questions through NMR investigations of the I and I* forms of OMTKY3 and OMIPF3. Information about structure was derived from measurements of NMR chemical shift changes and trans-hydrogen-bond *J*-couplings; information about dynamics was obtained through measurements of ^{15}N relaxation rates and $^{1}H-^{15}N$ heteronuclear NOEs with model-free analysis of the results. Although the I* forms of each variant are more dynamic than the corresponding I forms, the study revealed no appreciable difference in the backbone dynamics of either intact inhibitor (OMIPF3 vs OMTKY3) or modified inhibitor (OMIPF3* vs OMTKY3*). Instead, changes in chemical shifts and trans-hydrogen-bond *J*-couplings suggested that the $K_{hyd}°$ difference arises from differential intramolecular interactions within the intact inhibitors (OMIPF3 vs OMTKY3) in a region of each protein that becomes disordered upon reactive site cleavage (to OMIPF3* and OMTKY3*).

The steps leading to the hydrolysis and resynthesis of the reactive site peptide bond of a standard mechanism protein inhibitor can be written in simplified form as (*2*)

$$E + I \underset{k_{off}}{\overset{k_{on}}{\rightleftharpoons}} C \underset{k_{on}^*}{\overset{k_{off}^*}{\rightleftharpoons}} E + I^* \qquad (1)$$

where E is the enzyme and C is the stable complex between enzyme and inhibitor and I and I* are, respectively, the intact inhibitor and the modified (reactive site hydrolyzed) inhibitor. The hydrolysis constant K_{hyd} is defined as $K_{hyd} = I^*/I$, where I and I^* are, respectively, the concentrations of the intact and modified protein. Although a small, catalytic amount of proteinase is needed to reach equilibrium in a reasonable amount of time, the hydrolysis constant depends solely on the properties of the intact (I) and modified inhibitor (I*). The pH dependence of K_{hyd} is given by (*2*)

$$K_{hyd} = K_{hyd}° (1 + [H^+]/K_1 + K_2/[H^+]) \qquad (2)$$

where $K_{hyd}°$ is the equilibrium constant for the reaction where the newly formed carboxyl terminal is deprotonated and the newly formed amino-terminal is protonated and K_1 and K_2 are, respectively, the ionization constants of the newly formed carboxyl and alkylammonium groups. Equation 2 holds insofar as there are no significant perturbations of other ionizable groups in the protein as a consequence of the cleavage reaction.

‡ The assigned chemical shifts, coupling constants, and relaxation data have been deposited at BioMagResBank ⟨http:www.bmrb.wisc.edu⟩ under acquisition codes bmr5518 (OMTKY3), bmr5519 (OMTKY3*), bmr5520 (OMIPF3), and bmr5521(OMIPF3*).

* To whom correspondence should be addressed. Phone: +1 (608) 263-9349. Fax: +1 (608) 262-3759. E-mail: markley@nmrfam.wisc.edu.

[1] Abbreviations: CSA, chemical shift anisotropy; DSS, 4,4-dimethyl-4-silapentane-1-sulfonate, *E. coli*, *Escherichia coli*; K_{hyd}, hydrolysis constant for the cleavage reaction at the reactive site of a protein proteinase inhibitor; $K_{hyd}°$, pH-independent component of K_{hyd}; NOE, nuclear Overhauser enhancement; OMTKY3, third domain of the proteinase inhibitor (ovomucoid) from turkey (*Meleagris gallopavo*) consisting of residues 130−185 of whole ovomucoid (Swiss-Prot P01004); R_1, spin-latter ice relaxation rate; R_2, spin−spin relaxation rate; rCMTI-V, recombinant *Cucurbita maxima* trypsin inhibitor-V; R_{ex}, chemical exchange contribution to the decay of transverse magnetization during the CPMG pulse train; S^2, order parameter; S_f^2, order parameter for faster motions for cases in which two time scales are required; S_s^2, order parameter for slower motions for cases in which two time scales are required; SNase, staphylococcal nuclease; T_1, spin−lattice relaxation time; T_2, spin−spin relaxation time; τ_e, effective correlation time; τ_m, overall molecular tumbling correlation time. The Schecter-Berger (*1*) nomenclature is used to specify residue positions relative to the reactive site peptide bond (P_1 is the residue whose side chain is recognized by the specificity pocket of the proteinase; residues P_n are to the N-terminal side of the cleavage site; residues P_n' are to the C-terminal side).

10.1021/bi034041u CCC: $25.00
Published on Web 04/16/2003

Turkey ovomucoid third domain (OMTKY3) is a Kazal-type inhibitor of serine proteinases (*3*, *4*). It inhibits chymotrypsin-like enzymes in a standard, substrate-like manner. The pH-independent hydrolysis constant of OMTKY3, $K_{hyd}°$, has been determined to be unity at neutral pH (*2*), indicating not only that the intact and modified inhibitors have equivalent free energies, but that they also have equivalent association constants with the enzyme. Nevertheless, the denaturation temperature of a modified inhibitor is always lower than that of its intact form (*5*). In addition, the ratios k_{on}/k_{on}* and k_{off}/k_{off}* are normally large and vary with the identity of the proteinase (*5*). Inhibition by a modified inhibitor frequently is kinetically slow.

Structures of intact and reactive site modified OMTKY3 and some other ovomucoid third domains of the Kazal family have been determined in solution (*6*−*8*) and in crystals (*9*−*15*). Solution structures of OMTKY3 and OMTKY3* have shown that, upon reactive site peptide bond cleavage, the residues immediately at the clip site are less constrained and have fewer contacts with the main body of the protein. However, structures of other segments of the reactive site loop and the scaffolding region (protein core) remain rigid. In crystal structures of OMSVP3* (reactive site cleaved silver pheasant ovomucoid third domain) and OMJPQ3* (reactive site cleaved Japanese quail ovomucoid third domain) (*14*), the charged end-groups do not form ion pairs with one another. In modified inhibitors, the H-bond observed in intact inhibitors between the side chains of P_2-Thr^{17} and P_1'-Glu^{19} is broken, and the H-bonds between the P_{15}'-Asn^{33} side chain and the backbone carbonyl groups of P_2-Thr^{17} and P_1'-Glu^{19} are absent or weak. The stacking of the side chains of P_2'-Tyr^{20} and P_4'-Pro^{22}, present in intact inhibitors, is preserved in the modified inhibitors and may help stabilize the newly formed N-terminal peptide (residues 19−23) and lower the $K_{hyd}°$ of the inhibitor.

This investigation had two goals: (1) to investigate the physical basis for the very small $K_{hyd}°$ for OMTKY3 and (2) to understand the structural or dynamic origin of the change in $K_{hyd}°$ resulting from a single amino acid replacement at residue 20. OMTKY3 ($K_{hyd}° = 1.0$) has P_2'-Tyr^{20}, and Indian peafowl ovomucoid third domain (OMIPF3, $K_{hyd}° = 5.14$) has P_2'-His^{20} (*2*). Investigations of the structural or dynamic origins of thermodynamic differences as small as this (∼1 kcal/mol) are highly challenging (*16*, *17*). Our approach was to utilize newer NMR methods for determining protein dynamics (*18*, *19*) and hydrogen bonding (*20*, *21*).

EXPERIMENTAL PROCEDURES

Protein Expression and Purification. As described elsewhere (*22*), OMTKY3 was produced from *Escherichia coli* BL21(DE3) pLysS cells grown on a minimal medium; the expression plasmid coded for the fusion protein with OMTKY3 linked to staphylococcal nuclease with an engineered cyanogen bromide (CNBr) cleavage site in the linker between the two proteins. The methionines originally present in staphylococcal nuclease were converted to alanines to remove additional CNBr cleavage sites (*23*). To produce the P_2'-Tyr^{20}His variant (OMIPF3), the gene coding for OMTKY3 was modified appropriately by site-directed mutagenesis. The isolation and purification procedures were as described previously (*22*) with slight modification. In short, after cell harvest and lysis, inclusion bodies were separated by centrifugation.

Fusion protein was isolated from the cell pellet under denaturing conditions by the following procedure. The inclusion bodies, which had been washed several times with lysis buffer (50 mM Tris, 100 mM NaCl, pH 7.6) containing 1% (v/v) Triton X-100, were dissolved in 6 M GdmCl in the presence of 100 mM DTT for 2 h. The insoluble cell debris was removed by centrifugation, and the clear supernatant was dialyzed three times against 20 mM acetic acid. The dialyzed solution was centrifuged to remove precipitate, and the protein was renatured by rapid dilution of the supernatant into 50 mM Tris buffer containing 1.74 mM β-mercaptoethanol.

The purified fusion protein was dissolved in 0.1 M HCl, and cleavage was initiated by addition of a 30-fold molar excess of CNBr. The reaction mixture was covered with aluminum foil and incubated at room temperature in the hood for 4 h with gentle mixing. Excess CNBr was removed by lyophilization 4−5 times with double-distilled H_2O. The protein of interest was separated from SNase by elution with a gradient of 10% to 70% acetonitrile on a C18 reverse-phase HPLC column. For uniform $^{13}C/^{15}N$ or ^{15}N labeling, the host cells were grown on ^{13}C-glucose as the sole carbon source and/or ^{15}N-ammonium chloride as the sole nitrogen source.

Conversion of Intact Inhibitor to Modified Inhibitor. Intact forms of OMTKY3 and OMIPF3 were converted to OMTKY3* and OMIPF3* by methods described before (*2*, *24*) with minor modifications. The intact inhibitor was dissolved at a concentration of 2−3 mM in 1.5×10^{-2} M HCl; the final pH of the solution was adjusted with 1 M HCl to pH 1.5 for OMTKY3 and 1.9 for OMIPF3. Pronase (Calbiochem, CA) was then added to a final concentration of 1 mg/mL. The mixture was stirred gently at room temperature for 24−48 h. The cleavage reaction as monitored by [^1H,^{15}N]-HSQC NMR spectroscopy was judged to be 90% complete. The progress of the reaction was followed by monitoring the intensities of the $^{15}N^{\delta 2}-^1H^{\delta 21}$ and $^{15}N^{\delta 2}-^1H^{\delta 22}$ cross-peaks from P_{15}'-Asn^{33}, which exhibit distinct chemical shifts in the intact and the modified form of the inhibitors (*24*). After the reaction, the digestive enzymes were removed by chromatography on a Sephadex G-50 column (1×50 cm) preequilibrated with 0.02 M HCl. OMTKY3* and OMIPF3* were then desalted and separated from their intact forms on a reversed phase C18 HPLC column.

NMR Sample Preparation and Data Collection. Protein samples labeled uniformly with ^{15}N or $^{15}N+^{13}C$ were dissolved at a concentration of 1−2 mM in 90% H_2O/10% D_2O containing 100 mM KCl. Data were collected at two pH values: 6.0 and 3.9. All NMR spectra were recorded at 25 °C on Bruker spectrometers equipped with triple resonance probes (^1H, ^{13}C, ^{15}N, with ^2H lock) and *z*- or three-axis pulse field gradient capabilities. Quadrature detection in the indirectly detected dimensions was obtained either by the echo-antiecho or States-TPPI method (*25*). ^1H chemical shifts were determined relative to the internal reference, sodium 2,2-dimethyl-2-silapentaine-5-sulfonate (DSS), while the ^{15}N and ^{13}C chemical shifts were indirectly referenced to DSS (*26*).

^{15}N T_1 and T_2 and ^1H,^{15}N NOE measurements, for the intact and modified forms of each inhibitor at pH 6.0 taken at three

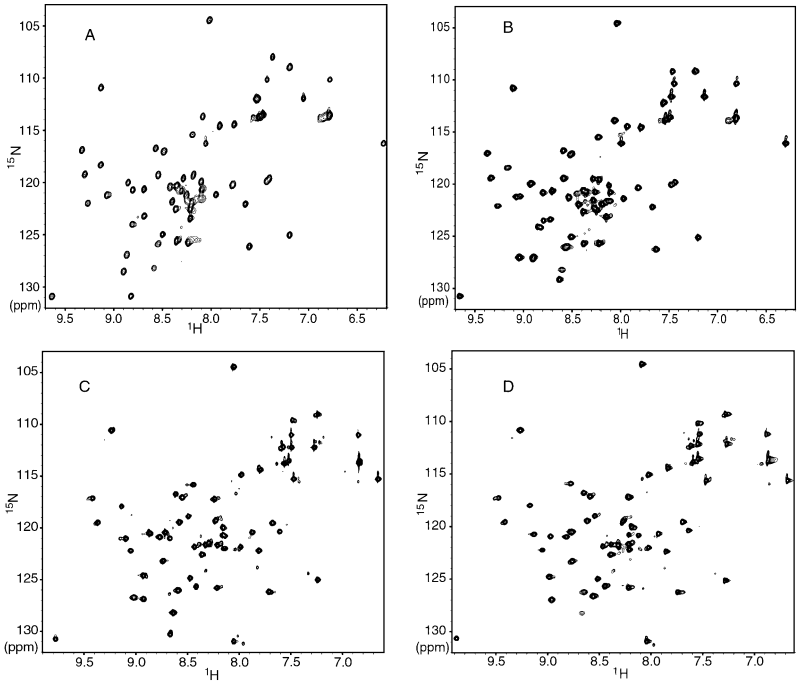

FIGURE 1: [^{1}H,^{15}N]-HSQC spectra of 1−2 mM protein samples at pH 6.0: (a) OMTKY3, (b) OMIPF3, (c) OMTKY3*, and (d) OMIPF3*.

magnetic field strengths (^{1}H frequencies: 750.13, 600.13, and 499.84 MHz) and for each modified inhibitor at pH 3.9 taken at two field strengths (750.13 and 600.13 MHz), were analyzed to obtain generalized order parameters (S^2), effective correlation times for internal motion (τ_e) of backbone NH vectors, and chemical exchange terms (R_{ex}). The pulse sequences used were those described by Farrow et al. (*18*) with a slight modification to include water flip-back (*27*) and 3-9-19 WATERGATE (*28*) techniques for eliminating the water resonance. At each magnetic field strength, nine data sets were collected to measure ^{15}N T_1, and eight data sets were collected to measure ^{15}N T_2. The delay values for the ^{15}N T_1 measurements were as follows: (750.13 MHz ^{1}H) 0, 10, 100, 200, 400, 600, 800, 1100, and 1500 ms; (600.13 MHz ^{1}H) 0, 10, 100, 200, 400, 600, 800, 1000, and 1400 ms; (499.84 MHz ^{1}H) 0, 10, 100, 200, 300, 500, 700, 900, 1100, and 1400 ms. The delay values for ^{15}N T_2 measurements were as follows: (750.13 MHz ^{1}H) 0, 24, 48, 72, 96, 144, 192, and 240 ms; (600.13 MHz ^{1}H) 0, 24, 48, 72, 96, 144, 184, and 256 ms; (499.84 MHz ^{1}H) 0, 24, 56, 88, 128, 176, 224, and 280 ms. In each data series, one or two duplicate spectra were collected for the purpose of error estimates. For the ^{1}H−^{15}N steady-state heteronuclear NOE measurements, two spectra, acquired with or without proton presaturation, were recorded in an interleaved manner.

Trans-hydrogen-bond $^{3h}J_{NC'}$ connectivities were measured by collecting 2D long-range TROSY-H(N)CO data sets (*21*) at 750.13 MHz ^{1}H and 2D long-range H(N)CO data sets (without the TROSY scheme) (*29*) at 500.13 MHz ^{1}H. The $^{3h}J_{NC'}$ values were derived from the spectra as described by Cordier and Grzesiek (*20*). The error estimates are the standard deviations derived from the results of two independent experiments.

Analysis of the Relaxation Parameters. NMR spectra were processed with Felix95 software (Molecular Simulations Inc., San Diego, CA) and analyzed with the Sparky software package (http://www.cgl.ucsf.edu/home/sparky). Intensities of cross-peaks were obtained from peak-picking routines provided in the software package. The parameter-fitting module in Sparky was used to determine ^{15}N T_1 and T_2 values by nonlinear least-squares fitting of experimental intensities for each peak to a single-exponential decay; these values were inverted to obtain ^{15}N R_1 and R_2 values, respectively. The reported error estimates are the standard deviations derived from the data fittings. ^{1}H−^{15}N steady-state heteronuclear NOEs were calculated from ratios of experimental peak heights: the heights of peaks from spectra with proton irradiation during the recycling delay divided by those from spectra without proton irradiation during the recycling delay. Uncertainties in peaks heights were assessed from RMS baseline noise levels. Repeated measurements of ^{15}N T_1 and T_2 relaxation values and heteronuclear NOEs were averaged. ^{15}N relaxation parameters were analyzed within the extended model-free framework (*30*−*32*) by using the program ModelFree v. 4.0 (*33*). The difference between the parallel and perpendicular components of the ^{15}N chemical shift tensor was taken to be −160 ppm (*34*). To account for the variability in the ^{15}N CSA (*35*) and systematic errors in measurements of T_2 (*36*), the uncertainties for those R_1 and R_2 whose initial error estimates were below 7% were set to 7% of their values.

RESULTS

Chemical Shift Assignments. [^{1}H, ^{15}N]-HSQC spectra of OMTKY3, OMIPF3, OMTKY3*, and OMIPF3* samples, all at pH 6.0, are compared in Figure 1. The presence of single strong peaks for each residue for OMTKY3 and OMIPF3 and strong peaks with only minor cross-peaks for OMTKY3* and OMIPF3* is consistent with each protein adopting a single major stable conformation.

Backbone ^{1}H, ^{15}N, and ^{13}C′ chemical shift assignments for OMTKY3 at pH 6.0 were determined from published values obtained at a variety of pH values (*37*−*39*). Most of the resonances of OMIPF3, which differs from OMTKY3 by only one residue (P_2'-Tyr^{20}His), could be assigned on the

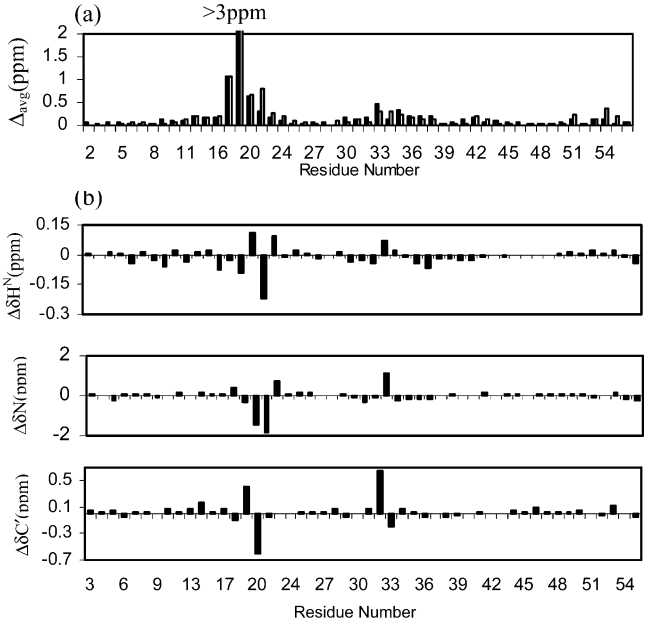

FIGURE 2: (a) Weighted average amide NH chemical shift differences as a function of residue number for (black bars) OMTKY3* vs OMTKY3 and (white bars) OMIPF3* vs OMIPF3. (b) Differences at pH 6.0 between the ^{1}H, ^{15}N, and ^{13}C′ chemical shifts of OMTKY3 and OMIPF3.

basis of their similarity to those of OMTKY3. Those that could not be determined in this way were assigned by combined analysis of ^{15}N edited [^{1}H,^{1}H]-TOCSY and [^{1}H,^{1}H]-NOESY data sets. The backbone ^{1}H and ^{15}N resonances of OMTKY3* and OMIPF3* were also assigned in this manner, with advantage taken of published ^{1}H NMR assignments for OMTKY3* (*24*). Assignments for all four proteins are listed in Supporting Information Table S1 and have been deposited at BMRB.

Chemical Shift Changes upon Modification. The weighted average chemical shift deviations for each ^{1}H/^{15}N pair, Δ_{avg}-(NH), between intact and modified inhibitors were calculated as described by Garrett et al. (*40*), where $\Delta_{avg}(NH) = \{[(\Delta\delta_H)^2 + ((\Delta\delta_N)/5)^2]/2\}^{1/2}$. The ^{1}H−^{15}N cross-peak from P_2'-His^{20} in OMIPF3* could not be observed at pH 6.0, owing to rapid exchange with solvent; instead, the chemical shifts of P_2'-His^{20} determined at pH 3.9 were used for the comparison ($\delta^1H^N = 9.14$ ppm and $\delta^{15}N = 122.9$ ppm). As shown in Figure 2a, the largest chemical shift changes upon cleavage are confined to the residues around the reactive site. In addition, sizable chemical shift changes were observed for residues in the α-helix and C-terminal regions of the inhibitors that lose contacts with the reactive site loop upon cleavage. As an example, upon cleavage the $^1H^{\delta21}$ and $^1H^{\delta22}$ signals of P_{15}'-Asn^{33} shift closer by 0.9 ppm in OMIPF3/OMIPF3* and 1.0 ppm in OMTKY3/OMKTY3*; these shifts can be accounted for by the loss of H-bonds between the side chain amide group of P_{15}'-Asn^{33} and backbone oxygens of P_2-Thr^{17} and P_1'-Glu^{19}. Residues to the C-terminal side of the cleavage site exhibited nearly identical chemical shift perturbations in OMTKY3/OMTKY3* and OMIPF3/OMIPF3*, whereas residues immediately N-terminal to the clipped site exhibited larger chemical shift perturbations in OMIPF3/OMIPF3* than in OMTKY3/OMTKY3*. P_{36}'-Gly^{54}, which according to crystallographic studies (*14*) forms H-bond with P_4'-Pro in both intact and modified inhibitor, also exhibited a slightly higher chemical shift deviation in OMIPF3/OMIPF3* than in OMTKY3/OMTKY3*.

Chemical Shift Changes Resulting from the Replacement Tyr^{20}His. As indicated by comparisons of the $^1H^N$, ^{15}N, and ^{13}C′ chemical shifts of OMTKY3 and OMIPF3 (Figure 2b), the most extensive backbone chemical shift changes between OMTKY3 and OMIPF3 occur in the segment P_1'-Glu^{19}−P_5'-Leu^{23}. Upon replacement of P_2'-Tyr^{20} by histidine, the amide nitrogen of P_3'-Arg^{21} shifts downfield by 1.8 ppm, and the carbonyl carbon of P_1'-Glu^{19} shifts upfield by 0.4 ppm. In addition, large chemical shift changes were also observed for the carbonyl carbon of P_{13}'-Gly^{32} ($|\Delta\delta C'| = 0.5$ ppm) and the amide group of P_{14}'-Asn^{33} ($|\Delta\delta N| = 1.0$ ppm). No appreciable backbone chemical shift perturbations were detected for residues in other parts of the primary loop and the core regions of OMTKY3 and OMIPF3.

^{15}N Relaxation Data and Order Parameters at pH 6.0. Relaxation parameters were measured for all the expected 52 backbone amide resonances in the intact forms of OMTKY3 and OMIPF3 (all but the N-terminal P_{18}-Leu^1 and the three prolines). In OMTKY3*, relaxation parameter measurements were carried out for all the expected 51 backbone amides (all those from OMTKY3 less the new N-terminal residue P_1'-Glu^{19}). In OMIPF3*, reliable quantification of peaks intensities was obtained for only 49 backbone amide resonances, as the resonance for P_2'-His^{20} was missing and that for P_5'-Leu^{23} overlapped the signal from P_{10}-Ser^9.

The data analysis assumed an axially symmetric diffusion model for all the proteins. NMR structures of OMTKY3 (*6*) and OMTKY3* (*8*) were used as the coordinate frames for intact forms and modified forms of inhibitors. Axial diffusion tensors were initially estimated by the software package QUADRIC_DIFFUSION (A. G. Palmer, Columbia University). Residues for which NOE < 0.65 at 600.13 MHz ^{1}H were excluded from consideration for this analysis, owing to possible fast internal motions or conformational exchange on the sub-ms scale (*41*). Furthermore, the criterion (*42*)

$$\frac{\langle T_2\rangle - T_{2,i}}{\langle T_2\rangle} - \frac{\langle T_1\rangle - T_{1,i}}{\langle T_1\rangle} < 1.5 \times \mathrm{SD} \qquad (3)$$

was applied to the remaining residues, where SD is the standard deviation of the collection of values of the left side for all residues considered at each field.

Using the initial estimates of the diffusion tensor resulting from the quadratic analysis, a model was selected for each residue of each protein, according to the procedure described by Mandel et al. (*43*). Relaxation data from most of the residues in the four proteins were fitted best by the one-parameter model (model 1, S^2) or two-parameter models (model 2, S^2 and τ_e; or model 3, S^2 and R_{ex}, where R_{ex} is slow-motion "chemical exchange" contribution). Residues in the N-terminal tails (P_{17}-Ala^2 to P_{13}-Val^6) required the three-parameter model (model 5: S_f^2, S_s^2, and τ_e, where S_f^2 is the order parameter for faster motions and S_s^2 is the order parameter for slower motions) or were not fitted adequately by any of the models. For residue P_2'-Tyr^{20} in OMTKY3*, only two reliable relaxation parameters (^{15}N R_1 and ^{1}H,^{15}N-NOE at 750.13 MHz) were available, and these could not be fitted to any of the models. In the final optimization of

Table 1: Average Order Parameter Values for Secondary Structural Elements of the Four Proteins: OMTKY3, OMTKY3*, OMIPF3, and OMIPF3[a]

structural element	residues considered	turkey ovomucoid third domain		Indian peafowl third domain	
		OMTKY3	OMTKY3*	OMIPF3	OMIPF3*
α	34−43	[10] 0.92 (0.02)	[10] 0.91 (0.03)	[10] 0.90 (0.04)	[10] 0.90 (0.03)
β1	23−25	[3] 0.87 (0.05)	[3] 0.86 (0.05)	[3] 0.85 (0.04)	[2] 0.86 (0.07)
β2	30−31	[2] 0.85 (0.03)	[2] 0.83 (0.02)	[2] 0.82 (0.01)	[2] 0.82 (0.02)
β3	50−53	[4] 0.89 (0.02)	[4] 0.86 (0.02)	[4] 0.88 (0.06)	[4] 0.87 (0.03)
reactive site loop residues	6−16	[9] 0.81 (0.11)	[9] 0.79 (0.10)	[9] 0.82 (0.09)	[8] 0.75 (0.12)
reactive site loop residues	17−21	[5] 0.83 (0.08)	[3] 0.49 (0.17)	[5] 0.84 (0.07)	[3] 0.46 (0.22)
turn (I)	26−29	[4] 0.92 (0.03)	[4] 0.91 (0.04)	[4] 0.89 (0.04)	[4] 0.89 (0.04)
turn (II)	32−33	[1] 0.88	[2] 0.89 (0.02)	[1] 0.91	[2] 0.90 (0.01)
turn (III)	44−49	[6] 0.85 (0.05)	[6] 0.85 (0.05)	[6] 0.83 (0.05)	[6] 0.83 (0.05)

[a] The numbers in square brackets indicate number of residues for which data were available; values in parentheses are error estimates.

the diffusion tensor, residues from the five N-terminal residues were excluded in order to avoid adverse effects from their increased local mobility. Powell minimization was used for the final optimization.

The molecular symmetry of OMTKY3* is highly similar to that of OMTKY3. On the basis of their solution structures, a relative ratio of 1:0.84:0.71 was determined for the principal moments of the inertia tensor of OMTKY3, and a relative ratio of 1:0.86:0.76 was determined for those of OMTKY3*. For OMTKY3, the optimized correlation time for overall tumbling, τ_m, was 3.6 ns with a diffusion anisotropy $D_{||}/D_{\perp} = 1.1$; for OMTKY3*, $\tau_m = 3.5$ ns with $D_{||}/D_{\perp} = 0.89$. For OMIPF3, $\tau_m = 3.5$ ns with $D_{||}/D_{\perp} = 1.2$; for OMIPF3*, $\tau_m = 3.6$ ns with $D_{||}/D_{\perp} = 1.1$.

The average values of the order parameter S^2 determined with the designated model for each residue from P_{13}-Val[6] to P_{38}'-Cys[56] were 0.87 ± 0.07 for OMTKY3, 0.86 ± 0.07 for OMIPF3, 0.84 ± 0.12 for OMTKY3*, and 0.82 ± 0.13 for OMIPF3*. The order parameters indicate that the rigidities of the scaffolding region (from P_4'-Leu[22] to P_{38}'-Cys[56]) are comparable for all four proteins. Order parameters derived for the N-terminal residues were consistently lower than average in both the intact and modified forms of the inhibitors (Figure 3a). Fitting of the relaxation data for these residues required a two-time-scale spectral density function, which suggested that the N-terminal tail is disordered on a picosecond to nanosecond time scale. On the other hand, residues flanking the disulfide bridge (P_{11}-Cys[8]−P_{20}'-Cys[38]) exhibited more rigidity than did other residues in the reactive site loop. Order parameters greater than 0.87 were determined for P_{11}-Cys[8] and P_{10}-Ser[9] in both forms of each inhibitor. Internal mobility was observed for the reactive site, even in the intact inhibitors, as shown by lower than average order parameters for residues P_2-Thr[17] through P_3'-Arg[21] of both OMTKY3 and OMIPF3 (Table 1). P_1'-Glu required fitting by a two-time-scale spectral density function in both OMTKY3 and OMIPF3 (with $\tau_e = 1200 \pm 820$ ps in OMTKY3 and $\tau_e = 790 \pm 960$ ps in OMTKY3). Fitting of relaxation data for the P_2' site required two-parameter models (with $\tau_e = 43 \pm 16$ ps in OMTKY3 and $R_{ex} = 1.70 \pm 0.25$ s^{-1} in OMIPF3). The modified forms of the inhibitors exhibited more extensive internal motions, as shown by the order parameters determined for residues in the newly formed N-terminal residues (P_2-P_3'), which were far below the average. Fitting of the measured relaxation data for all of these residues required the two-time-scale spectral density

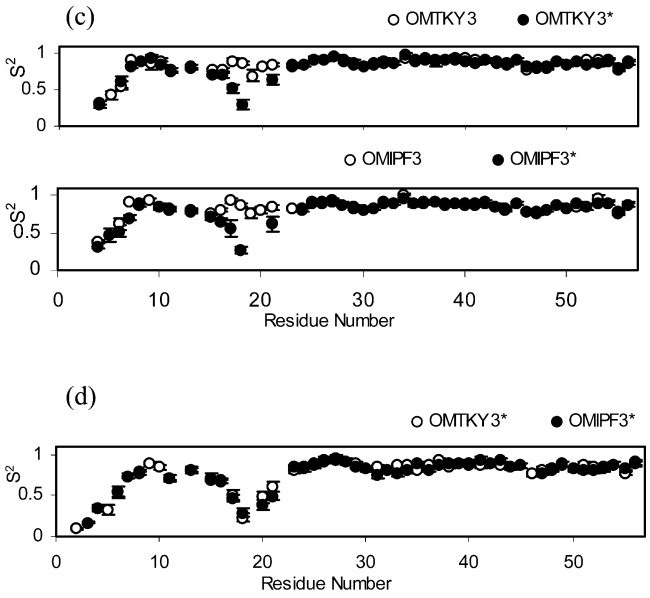

FIGURE 3: Order parameters ($S2$): (a) at pH 6.0 for OMTKY3, OMIPF3, OMTKY3*, and OMIPF3*; (b) at pH 3.9 for OMTKY3* and OMIPF3*.

function. The newly formed C-terminal residue, P_1-Leu[18], displayed the largest changes in mobility, with $S^2 = 0.2-0.3$ in the modified inhibitors compared with $S^2 = 0.86-0.87$ in the intact inhibitors. The order parameters for P_3'-Arg[21] were determined as 0.64 ± 0.05 in OMTKY3* and 0.62 ± 0.10 in OMIPF3*, lower than the values for the intact inhibitors by 0.22 and 0.23, respectively. The peptide amide group at the P_2'-site exhibited rapid hydrogen exchange with water, which resulted in very weak $^1H-^{15}N$ correlation peaks for P_2'-Tyr[20] of OMTKY3* and no observable peaks for P_2'-His[20] of OMIPF3*. Although none of the relaxation models adequately fitted data from P_2'-Tyr[20] in OMTKY3*, the ^{15}N R_1 (1.8 s^{-1}) and {^1H}-^{15}N NOE (0.61) values determined for this residue at ^1H 750.13 MHz were indicative of high disorder. Altered backbone mobility upon hydrolysis was also observed for other residues in the primary loop. For example, S^2, τ_e, and R_{ex} terms were required to fit the relaxation data for P_4-Ala[15] and P_3-Cys[16] in both OMTKY3* and OMIPF3*, while only S^2 terms were necessary to fit the relaxation data of these two sites in the intact inhibitors. However, no significant difference in local mobility was observed either between OMTKY3 and OMIPF3 or between OMTKY3* and OMIPF3*.

In both the intact and modified forms of the inhibitors, most of the residues that required τ_e parameters to fit the

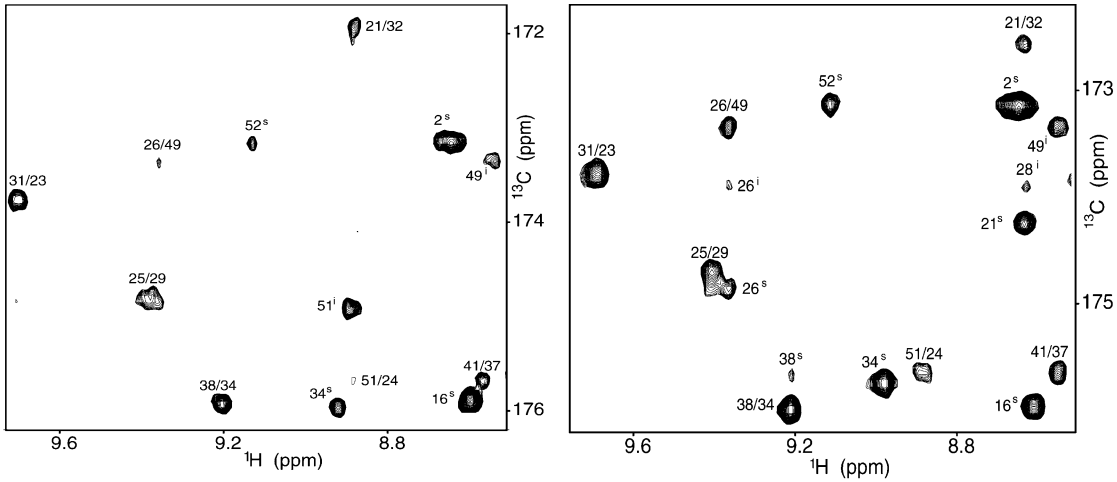

FIGURE 4: Comparable regions of long-range 2D H(N)CO spectra of (left) OMTKY3 and (right) OMIPF3. Trans-hydrogen-bond couplings $^{h3}J_{NC'}$ indicative of H-bonds are denoted by two numbers: the residue number of the amide H-bond donor followed by a slash and the residue number of the carbonyl H-bond acceptor. The superscript "s" denotes an incompletely suppressed sequential correlation between the ^{15}N nucleus of residue *i* and ^{13}C′ nucleus of residue $i - 1$, whereas the superscript "i" denotes an intraresidue $^{2}J_{NC'}$ correlation.

Table 2: Order Parameters of Reactive Site Loop Residues of OMTKY3* and OMIPF3* at pH 6.0 and pH 3.9[a]

	OMTKY3*		OMIPF3*	
residue	pH6.0	pH 3.9	pH 6.0	pH 3.9
P_4	0.71 (0.04)	0.69 (0.03)	0.73 (0.06)	0.72 (0.05)
P_3	0.70 (0.04)	0.69 (0.03)	0.66 (0.04)	0.67 (0.03)
P_2	0.52 (0.07)	0.50 (0.07)	0.56 (0.12)	0.47 (0.05)
P_1	0.30 (0.07)	0.23 (0.05)	0.27 (0.06)	0.29 (0.06)
P_2'		0.48 (0.08)		0.39 (0.06)
P_3'	0.64 (0.08)	0.61 (0.07)	0.62 (0.11)	0.50 (0.06)

[a] Numbers in parentheses are error estimates.

relaxation data were located in the reactive site loop and the loop between the α-helix and the third β-strand. In all the proteins, P_9-Glu[10] and P_{34}'-His[52] consistently required the R_{ex} parameter to fit the relaxation data.

^{15}N Relaxation Data and Order Parameters at pH 3.9. The relaxation data for OMTKY3* and OMIPF3* collected at pH 3.9 were analyzed in the same way as those collected at pH 6.0. For a given residue, the model providing the most reliable fit to the data was usually the same at each pH value. One of the few exceptions was P_1-Leu of OMTKY3*, which required only τ_e and S^2 at pH 3.9 but which required R_{ex}, τ_e, and S^2, at pH 6.0. The order parameters determined for each residue of OMTKY3* and OMIPF3* at pH 3.9 are compared in Figure 3b. For the data collected at pH 3.9, the average order parameter, calculated for residues P_{13}-Val[6] through P_{38}'-Cys[56], was 0.81 for OMTKY3* and 0.80 for OMIPF3*. Reliable relaxation parameters were determined at pH 3.9 for both P_2'-Tyr[20] in OMTKY3* and P_2'-His[20] in OMIPF3* through fitting to model 5. At this pH, the order parameters for the P_2' and P_3' sites were determined as 0.48 ± 0.08 and 0.61 ± 0.07, respectively, in OMTKY3* and 0.39 ± 0.06 and 0.50 ± 0.06, respectively, in OMIPF3* (Table 2). On the other side of the clipped site, each residue from P_{13}-Val[6] to P_1-Leu[18] yielded order parameters for OMTKY3* and OMIPF3* that were equivalent within experimental error. In addition, no significant differences in the rigidity of the scaffolding region were observed either between the two modified inhibitors at the lower pH or between the two modified inhibitors at both pH values.

Table 3: Three-Bond Trans-Hydrogen-Bond Couplings ($^{3H}J_{NC'}$) Determined for OMTKY3 and OMIPF3 at pH 6.0

		OMTKY3		OMIPF3	
donor	acceptor	$^{3h}J_{NC'}$ (Hz)	error (Hz)	$^{3h}J_{NC'}$ (Hz)	error (Hz)
R21 (N) (P_3')	G32 (O) (P_{14}')	0.654	0.022	0.478	0.026
L23 (N) (P_5')	Y31 (O) (P_{13}')	0.380	0.093	0.425	0.020
C24 (N) (P_6')	H52 (O) (P_{34}')	0.686	0.009	0.659	0.020
G25 (N) (P_7')	K29 (O) (P_{11}')	0.794	0.044	0.740	0.007
S26 (N) (P_8')	T49 (O) (P_{31}')	0.700	0.022	0.778	0.025
Y31 (N) (P_{13}')	L23 (O) (P_5')	0.814	0.015	0.798	0.026
F37 (N) (P_{19}')	N33 (O) (P_{15}')	0.332	0.001	0.405	0.033
C38 (N) (P_{20}')	K34 (O) (P_{16}')	0.776	0.016	0.757	0.013
N39 (N) (P_{21}')	C35 (O) (P_{17}')	0.338	0.038	0.249	0.031
V41 (N) (P_{23}')	F37 (O) (P_{19}')	0.565	0.009	0.490	0.007
V42 (N) (P_{24}')	C38 (O) (P_{20}')	0.409	0.017	0.387	0.005
S51 (N) (P_{33}')	C24 (O) (P_6')	0.490	0.030	0.462	0.041

$^{3h}J_{NC'}$ Trans-Hydrogen-Bond Connectivities. Comparable regions of long-range 2D H(N)CO spectra of OMKTY3 and OMIPF3 are shown in Figure 4. The full spectra contained 12 observable $^{3h}J_{NC'}$ connectivities for OMTKY3 and 14 for OMIPF3. The concentration of the OMIPF3 sample was slightly higher than that of OMTKY3 sample; this may account for observation of the two additional weak $^{3h}J_{NC'}$ cross-peaks, which corresponded to H-bonds between NH of P_{10}−Ser[9] and the side chain of P_{12}-Asp[7] and between NH of P_{23}'-Val[41] and the backbone oxygen of P_{19}'-Phe[37]. Only the 12 cross-peaks common to both molecules were included in the comparative analysis (Table 3). Of these, five represent H-bonds in the β-sheet (with average couplings: 0.63 ± 0.19 Hz in OMTKY3 and in 0.62 ± 0.17 Hz OMIPF3), and five represent in H-bonds in the α-helix (with average couplings of 0.48 ± 0.19 Hz in OMTKY3 and 0.46 ± 0.19 Hz in OMIPF3). The largest difference (Table 3) corresponded to the coupling between the NH of P_3'-Arg[21] and the backbone oxygen of P_{14}'-Gly[32], which was determined as 0.65 ± 0.02 Hz in OMTKY3 and 0.48 ± 0.03 Hz in OMIPF3. Slightly different couplings were determined for H-bonds between P_{23}'-Val[41] and P_{19}'-Phe[37], and between P_8'−Ser[26] and P_{31}'-Thr[49]. Values determined for the other $^{3h}J_{NC'}$ couplings in the two proteins were judged to be equivalent within experimental error.

DISCUSSION

Chemical Shifts of the Intact and Modified forms of OMTKY3 and OMIPF3 at pH 6.0. Changes in the chemical shifts of protein backbone atoms have been found to be reliable reporters of local structural and conformational changes (*44*−*51*). Differences in the chemical shifts of intact and modified OMTKY3 or OMIPF3 indicated that the major changes occur in residues near the cleavage site, P_2-Thr^{17}−P_2'-Arg^{21}, as expected from structural studies of OMTKY3* (*8*) and OMSVP3* (*14*). Additional appreciable chemical shift perturbations were observed for residues in the C-terminal part of the α−helix; these result from the weakening or disruption of noncovalent interactions between residues in this segment and residues in the reactive loop upon modification (*7*, *52*).

This study revealed that the backbone chemical shifts of P_{14}'-Gly^{32} and P_{15}'-Asn^{33} are altered by the single residue replacement at P_2'-site. According to the structure of OMTKY3 (*6*), it is very unlikely that these chemical shift perturbations arise exclusively from a direct electrostatic or ring current effect from the side chain of the substituted residue. Other residues close to the side chain of the P_2' residue exhibit only small chemical shift changes between OMTKY3 and OMIPF3 (for example 0.1 ppm for the side chain C^γ of P_{15}'-Asn^{33}). Instead, on the basis of trans-H-bond *J*-coupling measurements (discussed below), the chemical shift perturbations of the backbone resonances of P_{14}'-Gly^{32} and P_{15}'-Asn^{33} can be attributed to the changes in the strengths of hydrogen bonds.

Backbone Dynamics of the Intact and Modified forms of OMTKY3 and OMIPF3 at pH 6.0. The equivalent overall correlation times and average order parameters determined here for the intact and modified forms of OMTKY3 and OMTIPF3 are consistent with their comparable molecular weights and global structures. The sequential distributions of mean order parameters determined for the four proteins at pH 6.0 were also similar (Table 3). The average order parameters for the three most rigid regions of the four proteins were 0.90−0.92 for each helix, 0.89−0.92 for the P_8'-Ser^{26}−P_{11}'-Lys^{29} β-turn, and 0.88−0.91 for the P_{14}'-Gly^{32}−P_{15}'-Asn^{33} turn. Slightly lower order parameters were determined for the first β-strand (0.85−0.87) and the third β-strand (0.86−0.89). Still lower order parameters (0.82−0.85) were determined for the second β-strand and the loop between the α-helix and the third β-strand. The absence of a strict correlation between dynamics and secondary structure type has been noted in other proteins (*19*, *53*, *54*).

The N-terminal tail (P_{17}-Ala^2 to P_{14}−Ser^5) consistently exhibited the highest mobility in each protein. In none of the four proteins was it possible to fit relaxation data for P_{17}-Ala^2 or P_{16}-Ala^3 to any of the models; this probably is a consequence of anisotropic local motion in the N-terminal tail. The significantly lower than average order parameters determined for P_{15}-Val^4 and P_{14}-Ser^5 (0.30−0.50) are consistent with previous structural studies on OMTKY3 (*6*−*8*, *52*) as well as with results on the terminal regions of several other proteins (*18*, *19*, *54*−*56*). The C-terminal region was found to be well ordered, as expected from the disulfide linkage between P_6'-Cys^{24} and P_{38}'-Cys^{56} and the participation of these residues in third β-strand. The order parameter determined for the C-terminal residue P_{38}'-Cys^{56} in the four proteins (0.88−0.89) was slightly higher than the average values.

An R_{ex} term was consistently required for fitting of P_9-Glu^{10} and P_{34}'-His^{52} in all four proteins; this result suggests that both of these two residues undergo a local conformational fluctuation on the millisecond scale. In the solution structure of OMTKY3 (*7*), a transient intraresidue H-bond was proposed between the amide group and side chain carboxylate of P_9-Glu^{10}; it is possible that the making and breaking of this H-bond could be the source of the R_{ex} term determined for P_9-Glu^{10}.

In both inhibitors, the mobilities of residues P_2-Thr^{17} to P_3'-Arg^{21} in the reactive site loops were found to change significantly upon modification (Table 3), with the average order parameter for this stretch dropping from 0.83 ± 0.08 in OMTKY3 to 0.49 ± 0.17 in OMTKY3*, and from 0.84 ± 0.07 in OMIPF3 to 0.46 ± 0.22 in OMIPF3*. In analyzing the dynamics of the three residues at the active site (P_2, P_1 and P_3'), in the intact states only P_1 of OMIPF3 required two-parameter fitting (with $\tau_e = 100 \pm 37$ ps), whereas in the modified states of both inhibitors, all three sites required two-parameter fitting, with τ_e terms ranging from 400 ps to 1 ns. By contrast, residues P_{13}-Val^6−P_3-Cys^{16} in the primary loop showed no or only slight decreases in S^2 upon modification, with an average S^2 values of 0.81−0.82 in the intact inhibitors to 0.75−0.79 in the modified inhibitors. Nevertheless, slow conformational exchange was detected for residues P_4-Ala^{15} ($R_{ex} = 2.07 \pm 0.35$ s^{-1} in OMTKY3* and 1.75 ± 0.44 s^{-1} in OMIPF3*) and P_3-Cys^{16} ($R_{ex} = 0.85 \pm 0.25$ s^{-1} in OMTKY3* 0.80 ± 0.24 s^{-1} in OMIPF3*), whereas no R_{ex} term was required for either of these two residues in the intact inhibitors (OMTKY3 and OMIPF3).

It is known that cleavage of the reactive site peptide bond P_1—P_1' results in the disruption of many local interactions, including the H-bond between the side chains of P_1'-Glu^{19} and P_2-Thr^{17}, as well as the H-bonds between the backbone oxygens of P_1'-Glu^{19} and P_2-Thr^{17} and the side chain of P_{15}'-Asn^{33} (*14*). The enhanced mobility of the reactive site residues is believed to provide an entropic compensation for decrease in enthalpy resulting from the loss of the peptide bond in the modified inhibitor.

No significant differences in backbone mobility were observed, however, between the intact forms of the two inhibitors or between their modified forms (Table 1); the order parameters for all residues were equivalent within experimental error. In both intact inhibitors, P_1'-Glu exhibited similar internal motion in that fitting of the relaxation data for this residue required the two-time-scale spectral density function. Although the models chosen to fit the relaxation data for the P_1, P_2', and P_3' sites were slightly different between each inhibitor in the intact and modified states, the order parameters were comparable (Table S2). These results appear to rule out differences in mobility at the reactive site as being responsible for the difference in $K_{hyd}°$ between OMTKY3 and OMTKY3*.

Backbone Dynamics of the Reactive Sites of the Modified Inhibitors at pH 3.9. Because signals from the P_2' residue in the modified forms of the inhibitors were not resolved at pH 6.0, it was not possible to rule out differences in mobility at this site. For this reason, the dynamic parameters of OMTKY3* and OMIPF3* were investigated at pH 3.9,

which is slightly higher than the pK_a of the carboxyl terminal group of P_1-Leu in OMTKY3*. At this pH, hydrogen exchange of the backbone amide proton of the P_2' residue (Tyr[20] or His[20]) with solvent water is sufficiently slow that the $^1H-^{15}N$ cross-peaks are well resolved. At pH 3.9, as was the case at pH 6.0, there were no appreciable differences in the order parameters of corresponding residues of OMTKY3* and OMIPF3* either in the primary loop or the scaffolding region (Figure 3b). Overall, the dynamic properties of the reactive sites of OMTKY3* and OMIPF3* displayed by our studies were found to be indistinguishable both at pH 6.0 and pH 3.9. In conjunction with the comparison of backbone dynamics of OMTKY3 and OMIPF3 at pH 6.0, we conclude that the difference in $K_{hyd}°$ between the OMTKY3 and OMIPF3 cannot be explained by differences in their dynamics.

Analysis of Hydrogen Bonds. A precedent exists for the use of long range 2D H(N)CO measurements to monitor perturbed H-bond lengths in a protein (*29*, *57*). Cordier et al. (*29*) used this method to determine that the lengths of some of the H-bonds in the c-Src SH3 domain shorten upon ligand binding. Here we have used this approach to examine the H-bond network in OMTKY3/OMTKY3* and OMIPF3/OMIPF3* (Table 3). Only three of the twelve $^{3h}J_{NC'}$ connectivities compared by this method show significant changes between OMTKY3 and OMIPF3: changes larger than twice the error of the measurement. These correspond to the H-bonds between the H^N of P_3'-Arg[21] and the O of P_{14}'-Gly[32] ($\Delta^{3h}J_{NC'} = -0.176 \pm 0.048$ Hz), between the H^N of P_{19}'-Phe[37] and the O of P_{15}'-Asn[33] ($\Delta^{3h}J_{NC'} = 0.073 \pm 0.034$ Hz), and between the H^N of P_{23}'-Val[41] and the O of P_{19}'-Phe[37] ($\Delta^{3h}J_{NC'} = -0.075 \pm 0.016$ Hz). According to the correlation between $^{3h}J_{NC'}$ and H-bond length (*16*), two of the H-bonds lengthen and one shortens as a consequence of the substitution P_2'-Tyr[20]His. The effects on the two weaker H-bonds are opposite and essentially cancel one another. Thus, the net effect is close to that experienced by the strongest H-bond (that between H^N of P_3'-Arg[21] and O of P_{14}'-Gly[32]), which qualitatively corresponds to about a 20% weakening or 1 kcal/mol lower free energy for OMIPF3 relative to OMTKY3. Since this H-bond is broken in both OMIPF3* and OMTKY3*, this one change in H-bond strength would be sufficient to account for the observed difference in the $K_{hyd}°$ values of OMTKY3 and OMIPF3.

Comparison of the Backbone Dynamics of OMTKY3 and OMIPF3 with Those of Trypsin Inhibitor rCMTI-V. NMR spectroscopy has been used to investigate the internal mobilities of another proteinase inhibitor (recombinant *Cucurbita maxima* trypsin inhibitor-V, rCMTI-V) in its intact and modified states (*58*, *59*). The $K_{hyd}°$ for rCMTI-V has been determined to be around 9 at pH 6.75 (*60*). As with OMTKY3 and OMIPF3, considerable increases in local mobility were observed upon reactive site cleavage of rCMTI-V to rCMTI-V*. The newly formed C-terminal residues of rCMTI-V* (39−44) showed significantly decreased order parameters, whereas residues in the newly formed N-terminal tail remained as rigid as they were in the intact protein (*59*). The order parameters determined for the P_1 and P_2 residues of rCMTI-V* are comparable to those determined here for the P_1 and P_2 residues of OMTKY3* and OMIPF3*. Unlike those in OMTKY3* and OMIPF3*, the P_2' and P_3' residues of rCMTI-V* did not exhibit enhanced mobility. Then why does r-CMTI-V have a much higher $K_{hyd}°$ than OMTKY3? This question needs to be examined in terms of the contributions of both entropy and enthalpy to $K_{hyd}°$. In OMTKY3/OMTKY3*, the gain of entropy at P_3'-Arg[21] of OMTKY3* is probably compensated by a loss in enthalpy resulting from disruption of the H-bond between P_3'-Arg[21] and P_{14}'-Gly[32]. Furthermore, structures of OMTKY3 reveal a local H-bond network surrounding the scissile bond. The H-bond between the side chains of P_2-Thr[17] and P_1'-Glu[19], as well as the H-bonds between the backbone carbonyl oxygens of P_2-Thr[17] and P_1'-Glu[19] and the side chain carboxylate of P_{15}'-Asn[33] (*6*, *7*, *52*), helps hold the scissile bond P_1-P_1' intact. These H-bonds become broken after hydrolysis (*8*, *14*). By contrast in rCMTI-V/rCMTI-V*, which lacks this local H-bond network (*58*), there appears to be no compensating enthalpic term balancing the entropy gain upon cleavage of the reactive site peptide bond (*58*, *60*). In addition, the disulfide link between P_3-Cys[16] and P_{17}'-Cys[35] and the first β-strand (P_4'-Leu[23] to P_6'-Gly[25]) limit the propagation of increased mobility toward either side of the cleavage in OMTKY3* and OMIPF3*. N-terminal to the clipped site only residues P_2 and P_1 exhibit appreciable enhanced mobility, compared to the much broader range in the newly formed C-terminal tail of rCMTI-V* (*59*).

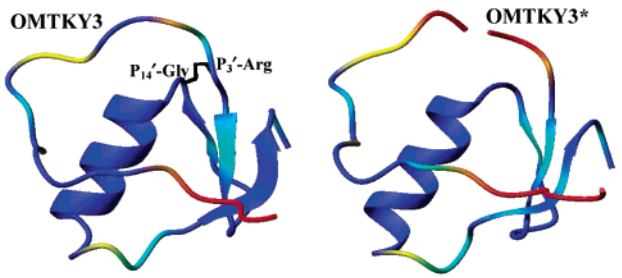

FIGURE 5: Dynamic properties of (left) OMTKY3 and (right) OMTKY3* displayed on their respective three-dimensional structures (*6*, *8*). The order parameter of each residue in OMTKY3 and OMTKY3* is indicated by a color scheme in which red represents $S^2 < 0.55$ (or unavailable because signals were not observed), orange represents $0.55 < S^2 \leq 0.7$, yellow represents $0.7 < S^2 \leq 0.8$, cyan represents $0.8 < S^2 \leq 0.85$, and blue represents >0.85. Depicted in black in the OMTKY3 structure is the H-bond between the H^N of P_3'-Arg[21] and the O of P_{14}'-Gly[32], which exhibited the largest $\Delta^{3h}J_{NC'}$ between OMKTY3 and OMIPF3; this H-bond is absent in the modified inhibitor (OMTKY3*).

CONCLUSIONS

Characterization of backbone dynamics, analysis of chemical shift perturbations, and measurements of trans-H-bond couplings has led to a more comprehensive understanding of the relative structures and dynamics of OMTKY3, OMTKY3*, OMIPF3, and OMIPF3*. Comparison of the dynamic properties of the modified inhibitors with those of their intact forms indicated that the reactive site becomes much more mobile upon hydrolysis (Figure 5). However, no appreciable difference in backbone dynamics was observed between either the intact or the modified forms of OMTKY3 and OMIPF3. Thus, changes in dynamics appear not to be responsible for the observed difference in $K_{hyd}°$ for turkey and Indian peafowl ovomucoid third domain (*2*). Instead, the H-bond between H^N of P_3'-Arg[21] and O of P_{14}'-Gly[32] was observed to be weaker by about 1 kcal/mol in OMIPF3 than in OMTKY3. Since this H-bond is broken both

OMIPF3* and OMTKY3*, the difference in free energy between OMIPF3 and OMTKY3 is sufficient, all other factors being equal, to account for the observed change in K_{hyd}° (Figure 5).

SUPPORTING INFORMATION AVAILABLE

Table S1 with complete assignments to the backbone amide groups and the side chain amides of asparagines for OMTKY3, OMTKY3*, OMIPF3, and OMIPF3* and Table S2 with complete values for the relaxation parameters for OMTKY3 at pH 6.0 are available free of charge via the Internet at http://pubs.acs.org.

REFERENCES

1. Schechter, I., and Berger, A. (1967) *Biochem. Biophys. Res. Commun. 27*, 157−162.
2. Ardelt, W., and Laskowski, M., Jr. (1991) *J. Mol. Biol. 220*, 1041−1053.
3. Bode, W., and Huber, R. (1992) *Eur. J. Biochem. 204*, 433−451.
4. Laskowski, M., Jr., and Kato, I. (1980) *Annu. Rev. Biochem. 49*, 593−626.
5. Laskowski, M., Qasim, M. A., and Lu, S. M. (2000) in *Protein−Protein Recognition* (Colin Kleanthous, Ed.) pp 228−279, Oxyford University Press, New York.
6. Hoogstraten, C. G., Choe, S., Westler, W. M., and Markley, J. L. (1995) *Protein Sci. 4*, 2289−2299.
7. Krezel, A. M., Darba, P., Robertson, A. D., Fejzo, J., Macura, S., and Markley, J. L. (1994) *J. Mol. Biol. 242*, 203-214.
8. Walkenhorst, W. F., Krezel, A. M., Rhyu, G.-I., and Markley, J. L. (1994) *J. Mol. Biol. 242*, 215−230.
9. Bode, W., Epp, O., Huber, R., Laskowski, M., Jr., and Ardelt, W. (1985) *Eur. J. Biochem. 147*, 387−395.
10. Bode, W., Wei, A. Z., Huber, R., Meyer, E., Travis, J., and Neumann, S. (1986) *EMBO J. 5*, 2453−2458.
11. Fujinaga, M., Read, R. J., Sielecki, A., Ardelt, W., Laskowski, M., Jr., and James, M. N. (1982) *Proc. Natl. Acad. Sci. U.S.A. 79*, 4868−4872.
12. Fujinaga, M., Delbaere, L. T., Brayer, G. D., and James, M. N. (1985) *J. Mol. Biol. 184*, 479−502.
13. Huang, K., Lu, W. Y., Anderson, S., Laskowski, M., Jr., and James, M. N. G. (1995) *Protein Sci. 4*, 1985−1997.
14. Musil, D., Bode, W., Huber, R., Laskowski, M., Jr., Lin, T. Y., and Ardelt, W. (1991) *J. Mol. Biol. 220*, 739−755.
15. Papamokos, E., Weber, E., Bode, W., Huber, R., Empie, M. W., Kato, I., and Laskowski, M., Jr. (1982) *J. Mol. Biol. 158*, 515−537.
16. Cornilescu, G., Ramirez, B. E., Frank, M. K., Clore, G. M., Gronenborn, A. M., and Bax, A. (1999) *J. Am. Chem. Soc. 121*, 6275−6279.
17. Yang, D., Mok, Y. K., Forman-Kay, J. D., Farrow, N. A., and Kay, L. E. (1997) *J. Mol. Biol. 272*, 790−804.
18. Farrow, N. A., Muhandiram, R., Singer, A. U., Pascal, S. M., Kay, C. M., Gish, G., Shoelson, S. E., Pawson, T., Forman-Kay, J. D., and Kay, L. E. (1994) *Biochemistry 33*, 5984−6003.
19. Kay, L. E., Torchia, D. A., and Bax, A. (1989) *Biochemistry 28*, 8972−8979.
20. Cordier, F., and Grzesiek, S. (1999) *J. Am. Chem. Soc. 121*, 1601−1602.
21. Wang, Y. X., Jacob, J., Cordier, F., Wingfield, P. T., Stahl, S. J., Lee-Huang, S., Torchia, D. A., Grzesiek, S., and Bax, A. (1999) *J. Biomol. NMR 14*, 181−184.
22. Hinck, A. P., Walkenhorst, W. F., Westler, W. M., Choe, S., and Markley, J. L. (1993) *Prot. Eng. 6*, 221−227.
23. Assadi-Porter, F. M., Aceti, D. J., Cheng, H., and Markley, J. L. (2000) *Arch. Biochem. Biophys. 376*, 252−258.
24. Rhyu, G. I., and Markley, J. L. (1988) *Biochemistry 27*, 2529−2539.
25. Marion, D., and Wüthrich, K. (1983) *Biochem. Biophys. Res. Comm. 113*, 967−974.
26. Wishart, D. S., Bigam, C. G., Yao, J., Abildgaard, F., Dyson, H. J., Oldfield, E., Markley, J. L., and Sykes, B. D. (1995) *J. Biomol. NMR 6*, 135−140.
27. Mori, S., Abeygunawardana, C., Johnson, M. O., and van Zijl, P. C. (1995) *J. Magn Reson. B 108*, 94−98.
28. Piotto, M., Saudek, V., and Sklenár, V. (1992) *J. Biomol. NMR 2*, 661−665.
29. Cordier, F., Wang, C. Y., Grzesiek, S., and Nicholson, L. K. (2000) *J. Mol. Biol. 304*, 497−505.
30. Clore, G. M., Szabó, A., Bax, A., Kay, L. E., Driscoll, P. C., and Gronenborn, A. M. (1990) *J. Am. Chem. Soc. 112*, 4989−4991.
31. Lipari, G., and Szabó, A. (1982) *J. Am. Chem. Soc. 104*, 4559−4570.
32. Lipari, G., and Szabó, A. (1982) *J. Am. Chem. Soc. 104*, 4546−4559.
33. Palmer, A. G., III, Rance, M., and Wright, P. E. (1991) *J. Am. Chem. Soc. 113*, 4371−4380.
34. Hiyama, Y., Niu, C., Silverton, J. V., Bavoso, A., and Torchia, D. (1988) *J. Am. Chem. Soc. 110*, 2378−2383.
35. Tjandra, N., Szabó, A., and Bax, A. (1996) *J. Am. Chem. Soc. 118*, 6986−6991.
36. Ross, A., Czisch, M., and King, G. C. (1997) *J. Magn. Reson. 124*, 355−365.
37. Choe, S., Dzakula, Z., Kuloglu, E. S., and Markley, J. L. (1998) *J. Biomol. NMR 12*, 193−195.
38. Robertson, A. D., Westler, W. M., and Markley, J. L. (1988) *Biochemistry 27*, 2519−2529.
39. Robertson, A. D., Rhyu, G.-I., Westler, W. M., and Markley, J. L. (1990) *Biopolymers 29*, 461−467.
40. Garrett, D. S., Seok, Y. J., Peterkofsky, A., Clore, G. M., and Gronenborn, A. M. (1997) *Biochemistry 36*, 4393−4398.
41. Tjandra, N., Feller, S. E., Pastor, R. W., and Bax, A. (1995) *J. Am. Chem. Soc. 117*, 12562−12566.
42. Tjandra, N., Wingfield, P. T., Stahl, S. J., and Bax, A. (1996) *J. Biomol. NMR 8*, 273−284.
43. Mandel, A. M., Akke, M., and Palmer, A. G., III (1995) *J. Mol. Biol. 246*, 144−163.
44. Clayden, N. J., and Williams, R. J. P. (1982) *J. Magn. Reson. 49*, 383−396.
45. Cornilescu, G., Delaglio, F., and Bax, A. (1999) *J. Biomol. NMR 13*, 289−302.
46. Dalgarno, D. C., Levine, B. A., and Williams, R. J. (1983) *Biosci. Rep. 3*, 443−452.
47. Markley, J. L., Meadows, D. H., and Jardetzky, O. (1967) *J. Mol. Biol. 27*, 25−40.
48. Spera, S., and Bax, A. (1991) *J. Am. Chem. Soc. 113*, 5490−5492.
49. Szilagyi, L., and Jardetzky, O. (1989) *J. Magn. Reson. 83*, 441−449.
50. Williamson, M. P. (1990) *Biopolymers 29*, 1423−1431.
51. Wishart, D. S., Sykes, B. D., and Richards, F. M. (1991) *J. Mol. Biol. 222*, 311−333.
52. Fujinaga, M., Sielecki, A. R., Read, R. J., Ardelt, W., Laskowski, M., Jr., and James, M. N. G. (1987) *J. Mol. Biol. 195*, 397−418.
53. Clore, G. M., Driscoll, P. C., Wingfield, P. T., and Gronenborn, A. M. (1990) *Biochemistry 29*, 7387−7401.
54. Stone, M. J., Chandrasekhar, K., Holmgren, A., Wright, P. E., and Dyson, H. J. (1993) *Biochemistry 32*, 426−435.
55. Kordel, J., Skelton, N. J., Akke, M., Palmer, A. G., III, and Chazin, W. J. (1992) *Biochemistry 31*, 4856−4866.
56. Stone, M. J., Fairbrother, W. J., Palmer, A. G., III, Reizer, J., Saier, M. H., Jr., and Wright, P. E. (1992) *Biochemistry 31*, 4394−4406.
57. Cordier, F., and Grzesiek, S. (2002) *J. Mol. Biol. 317*, 739−752.
58. Liu, J., Prakash, O., Cai, M., Gong, Y.-X., Huang, Y., Wen, L., Wen, J. J., Huang, J.-K., and Krishnamoorthi, R. (1996) *Biochemistry 35*, 1516−1524.
59. Liu, J., Prakash, O., Huang, Y., Wen, L., Wen, J. J., Huang, J.-K., and Krishnamoorthi, R. (1996) *Biochemistry 35*, 12503−12510.
60. Cai, M., Gong, Y.-X., Prakash, O., and Krishnamoorthi, R. (1995) *Biochemistry 34*, 12087−12094.

BI034041U